SCIENCE CHINA
Information Sciences

• RESEARCH PAPER •

November 2026, Vol. 69, Iss. 11, 212102:1–212102:16
https://doi.org/10.1007/s11432-024-5091-8

Two-stage instance selection domain adaptation for diagnostic classification of neuropsychiatric disorders

Minghao DAI, Jianpo SU, Zhipeng FAN, Limin PENG, Dewen HU & Ling-Li ZENG*

College of Intelligence Science and Technology, National University of Defense Technology, Changsha 410073, China

Received 24 October 2024/Revised 24 September 2025/Accepted 17 March 2026/Published online 16 October 2026

Abstract Neuropsychiatric disorders are particularly serious health issues that affect the cognitive ability, emotion and behavior of individuals. The increasing prevalence and severe symptoms reflect the urgent need for effective diagnostic classification methods for neuropsychiatric disorders. Recent studies combine multi-site functional magnetic resonance imaging (fMRI) data and domain adaptation techniques to address this problem. However, most related studies primarily focus on feature matching across the source and target domains, neglecting the issue of negative transfer brought by source data that exhibit low relevance with the target domain. In this study, we propose a two-stage instance selection domain adaptation algorithm (TS-ISDA) to tackle this issue. Specifically, we propose the minimum transfer distance (MTD) for direct distance measurement between a given sample and distribution. The MTD-based source instance selection and the target instance refinement steps are performed progressively to filter out unrelated source data and target instances with low-quality pseudo labels to ensure the effectiveness of the category-level feature alignment process. Then the local maximum mean discrepancy between the selected source and target data is calculated as the domain alignment loss. We conduct cross-site diagnostic classification studies of schizophrenia (SCZ), major depressive disorder (MDD) and autism spectrum disorder (ASD) based on fMRI data of 1003, 1043 and 607 participants from six sites, respectively. TS-ISDA achieves the highest average accuracies of 81.2%, 68.2% and 69.3% for SCZ, MDD and ASD, respectively, outperforming state-of-the-art methods. Furthermore, the discriminative brain regions identified by TS-ISDA show that the orbitofrontal cortex and the middle temporal gyrus regions consistently contribute significantly to the diagnosis of SCZ, MDD and ASD, guiding the search for biomarkers of various neuropsychiatric disorders.

Keywords domain adaptation, instance selection, negative transfer, distance metric, neuropsychiatric disorders, multi-site fMRI

Citation Dai M H, Su J P, Fan Z P, et al. Two-stage instance selection domain adaptation for diagnostic classification of neuropsychiatric disorders. Sci China Inf Sci, 2026, 69(11): 212102, https://doi.org/10.1007/s11432-024-5091-8

1 Introduction

Neuropsychiatric disorders are disorders of brain dysfunction caused by a combination of biological, psychological and social factors, which are clinically manifested as mental activity abnormalities in cognition, emotion and behavior [1]. According to statistics from the World Health Organization, nearly one billion people worldwide suffer from neuropsychiatric disorders, and the prevalence among adolescents is as high as 14%. Current clinical diagnostic methods for neuropsychiatric disorders are generally symptom-based and mainly rely on neuropsychological tests and decisions of medical professionals, which are highly subjective and less reliable. Therefore, there is still a lack of objective, effective and applicable methods for diagnostic classification of neuropsychiatric disorders.

Functional magnetic resonance imaging (fMRI) is a neuroimaging technique for indirect inference of brain activity from blood-oxygen-level-dependent (BOLD) signals. Previous evidence shows that fMRI-based deep learning techniques can be utilized to distinguish patients with neuropsychiatric disorders from normal people, and to discover reliable biomarkers [2–4]. Considering the limited fMRI data from a single site and the data heterogeneity issue across different sites [5], recent studies combine multi-site fMRI data and domain adaptation techniques for diagnostic classification of neuropsychiatric disorders [6–8]. But most relevant studies mainly concentrate on feature alignment across the source and target domains, lacking attention to the impact of unrelated source data on domain adaptation.

Current research on fMRI adaptation mainly confronts two issues. Domain adaptation is essentially knowledge transfer from the source domain to the target domain, and relies on the similarity between them. In diagnostic classification of neuropsychiatric disorders based on multi-site fMRI data, source instances that are less related to the target site (hard source samples) may bring a negative impact on the models' performance, i.e., negative transfer [9].

* Corresponding author (email: zengphd@nudt.edu.cn)

© Science China Press 2026

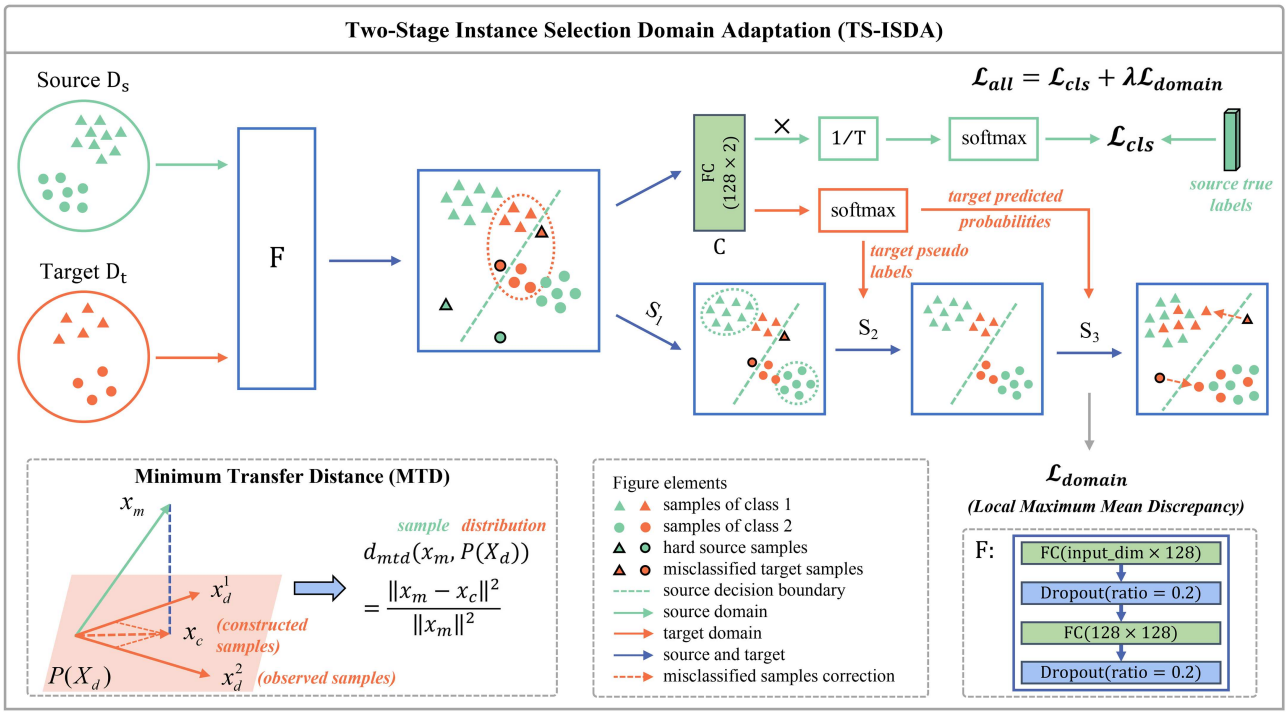


Figure 1 (Color online) Framework of the two-stage instance selection domain adaptation (TS-ISDA). TS-ISDA consists of three steps, S_1: MTD-based source instance selection, S_2: target instance refinement, S_3: local feature alignment. The MTD-based source instance selection and the target instance refinement steps are performed progressively to filter out unrelated source data and target instances with low-quality pseudo labels. Through the category-level feature alignment process, the misclassified target samples are automatically corrected to their correct classes. The cross entropy classification loss $\mathcal{L}_{cls}$ and the local maximum mean discrepancy between the selected source and target data $\mathcal{L}_{domain}$ are combined for model optimization. The calculation schema of MTD in low-dimensional space is also shown in this figure.

Therefore, these instances should be less weighted or discarded when performing domain adaptation. Most of the existing studies derive the relevance between source instances and the target distribution through outcomes of the domain classifier or adaptive weight learning in the optimization process [9–12], facing issues of imprecision and inexplicability. Besides, early domain adaptation studies focus on global domain alignment between the source domain and target domain. However, due to the inter-site distribution shift in multi-site neuroimaging data, global alignment approaches may cause distribution confusion across irrelevant subdomains [13, 14], thereby potentially compromising model performance. To avoid this issue, many studies propose to introduce category information to achieve fine-grained domain alignment [15–18]. Since the target domain has no labels in an unsupervised domain adaptation scenario, the pseudo labels of target samples generated by the source classifier are usually used for demarcation of subdomains. In that case, target samples with low-quality pseudo labels would misguide the domain alignment process, and degrade the diagnostic performance of learned models in the target site.

In this study, we propose the minimum transfer distance (MTD) for sample-distribution distance measurement. Based on MTD, we also propose a two-stage instance selection domain adaptation algorithm (TS-ISDA) to enhance cross-site diagnostic classification of neuropsychiatric disorders. The framework of TS-ISDA is shown in Figure 1. Specifically, we firstly perform MTD-based source instance selection to filter out unrelated source data, to help avoid the issue of negative transfer during the domain adaptation process. Then we perform target instance refinement to filter out target instances with low-quality pseudo labels for effective category-level domain alignment. Finally, the local maximum mean discrepancy between the selected source and target data is calculated as the domain alignment loss. Through the category-level feature alignment process, the misclassified target samples are automatically corrected to their correct classes. We conduct a large-scale cross-site diagnostic classification study of schizophrenia (SCZ), major depressive disorder (MDD) and autism spectrum disorder (ASD) based on fMRI data of 1003, 1043 and 607 subjects from six sites, respectively. TS-ISDA achieves the highest average accuracies of 81.2%, 68.2% and 69.3% for SCZ, MDD and ASD with the Cameron Craddock 200 ROI (CC200) brain atlas, respectively, outperforming state-of-the-art domain adaptation methods.

The major contributions of our study are reflected in three aspects.

(1) We propose MTD for direct distance measurement between the given sample and distribution, and perform MTD-based source instance selection to help avoid negative transfer in the domain adaptation process.

(2) We also propose to filter out target instances with low-quality pseudo labels to guarantee the effectiveness of the category-level feature alignment process.

(3) We propose a two-stage instance selection domain adaptation algorithm for fMRI-based cross-site diagnostic classification of neuropsychiatric disorders. Comprehensive experiments based on multi-site fMRI data of SCZ, MDD and ASD demonstrate the superiority and robustness of TS-ISDA compared to state-of-the-art methods.

The remainder of this paper is organized as follows. Section 2 briefly describes the recent research on domain adaptation and fMRI-based diagnostic classification of neuropsychiatric disorders. Methods, materials, experimental settings and results are introduced in Sections 3 and 4, respectively. Section 5 presents the conclusions of this study.

2 Related work

2.1 Domain adaptation through feature matching and instance reweighting

To better eliminate the distribution differences across the source and target domains, many studies propose to introduce category information to achieve finer domain alignment [15–18]. Kang et al. introduced the contrastive domain discrepancy and embedded it in the proposed contrastive adaptation network, to perform category-level domain alignment by minimizing the intra-class domain discrepancy and maximizing the inter-class domain discrepancy [19]. Chen et al. developed an easy-to-hard transfer scheme to filter out target samples with low-quality pseudo labels, and proposed an adaptive prototype alignment module to enforce the category-level domain alignment [20]. Most of these studies only focus on searching for an optimal feature alignment method across the source and target domains, lacking attention to the negative transfer issue brought by source data that exhibit low relevance with the target domain.

To address the issue of negative transfer during the domain adaptation procedure, some researchers conduct source instance reweighting when calculating the classification loss or domain alignment loss [9, 10]. Azarkesht et al. employed a dynamic importance weighted strategy to better align the marginal and conditional distributions across the source and target domains, and utilized the $L_{2,1}$-norm structured sparsity regularizer to adaptively learn weights for source instances [11]. Li et al. utilized the kernel mean matching method to reduce the marginal and conditional distribution differences between the source and target domains, while simultaneously amending weights for source instances based on their distances from the target instances [12]. However, the weights derived based on existing methods typically lack interpretability, and could not measure the relevance between source instances and the target distribution accurately.

2.2 FMRI-based diagnostic classification of neuropsychiatric disorders

Previous studies have proven that fMRI data can be utilized to distinguish patients with neuropsychiatric disorders and healthy controls [2–4]. Considering the limited data from one single site, many studies propose to combine fMRI data from multiple sites to enhance the generalization ability of classification models [21, 22]. However, different sites usually suffer from domain shifts caused by different data distributions. In that case, domain adaptation techniques are used to mitigate the domain shifts and improve the target performance of learned models. Wang et al. proposed a multi-source domain adaptation and multi-view sparse representation algorithm, which transforms all the source subjects into the same target feature space, and then a classifier for multi-class ASD classification is developed utilizing both views of the functional connectivity and functional correlation tensor features [6]. Kunda et al. introduced a domain adaptation module to eliminate the feature dependency on the site, and enhanced the identification accuracy of ASD by combining the tangent Pearson measure and phenotypic information [7]. Huang et al. utilized the conditional adversarial domain adaptation method to help the model learn site-invariant discriminative feature representations, and improved the fMRI-based diagnostic classification of attention-deficit hyperactivity disorder (ADHD) [8]. These studies primarily concentrate on extraction of domain-invariant feature representations, while ignoring the impact of unrelated source data on domain adaptation.

Compared with previous studies, we propose the MTD and perform MTD-based source instance selection to help avoid negative transfer in the domain adaptation process. Besides, we also propose to select target instances with reliable pseudo labels to guarantee the effectiveness of the category-level domain alignment process. The two steps are performed progressively and the local feature alignment process is carried out on the selected source and target data.

3 Methods

3.1 Formulation and notation

In an unsupervised domain adaptation scenario, there are a labeled source domain $\mathcal{D}_s = \{X_s, Y_s\} = \{(x_s^i, y_s^i)\}_{i=1}^{n_s}$ and an unlabeled target domain $\mathcal{D}_t = \{X_t\} = \{(x_t^j)\}_{j=1}^{n_t}$. In our task, domain shifts exist between the source domain and target domain due to different data distributions. Our goal is to reduce the feature distribution discrepancy between $\mathcal{D}_s$ and $\mathcal{D}_t$ with the minimum loss of task-related discriminative information, thus improving the generalization ability of learned models in the target domain.

3.2 Minimum transfer distance

Even though there are many valid distance metrics designed for sample-sample or distribution-distribution distance measurement, an effective sample-distribution distance measurement method is still lacking. We assume that the distance between the given sample and distribution is 0 if and only if this sample could be linearly represented by observed samples in the distribution. Based on this assumption, we propose the MTD to measure the distance between the given sample and distribution, and the calculation schema of MTD in low-dimensional space is shown in Figure 1. The detailed calculation process of MTD is introduced as follows.

Suppose that we are given one sample x_m and one distribution $P(X_d)$, where $X_d \in R^{n_d \times d}$ is the feature matrix of observed samples in distribution $P(X_d)$, where n_d and d respectively denote the number and feature dimension of these samples. The elements $x_d^i \in X_d$ $(i = 1, \ldots, n_d)$ represent the observed samples in distribution $P(X_d)$. In our proposed MTD, x_m shares the same feature dimension with x_d^i, i.e., $D(x_m) = d$, and the distance between the given sample and distribution is calculated based on x_m and x_d^i $(i = 1, \ldots, n_d)$. Since linear combinations of random variables from the same distribution still belong to this distribution, we firstly search for the linear combination of x_d^i $(i = 1, \ldots, n_d)$ that is closest to x_m. The coefficients of this linear combination can be derived by solving the following optimization problem:

$$l = \arg\min_{t \in R^{1 \times n_d}} \|x_m - t \cdot X_d\|^2. \tag{1}$$

We can calculate the constructed sample x_c with the combination coefficients l, i.e., $x_c = l \cdot X_d$. Since x_c is the sample closest to x_m in distribution $P(X_d)$, we can define the distance between x_m and x_c as the minimum transfer distance from x_m to $P(X_d)$, which is formulated as follows:

$$d_{mtd}(x_m, P(X_d)) = \frac{\|x_m - x_c\|^2}{\|x_m\|^2}. \tag{2}$$

3.3 Local maximum mean discrepancy

In a cross-domain classification scenario, distribution differences existing between the source domain and target domain seriously degrade the target performance of learned models. Local maximum mean discrepancy (LMMD) is a variant of maximum mean discrepancy (MMD), which measures the distance between relevant subdomains within the same category, and has been extensively utilized in discrepancy-based domain adaptation methods [15]. In practical applications, an unbiased estimate of LMMD is formulated as follows:

$$\begin{aligned}\hat{d}_{\mathcal{H}}^{l}(p,q) =& \frac{1}{C}\sum_{c=1}^{C}\left\|\sum_{i=1}^{n_p}\omega_i^{p(c)}\phi(x_i^p) - \sum_{j=1}^{n_q}\omega_j^{q(c)}\phi(x_j^q)\right\|_{\mathcal{H}}^2 \\ =& \frac{1}{C}\sum_{c=1}^{C}\left[\sum_{i=1}^{n_p}\sum_{j=1}^{n_p}\omega_i^{p(c)}\omega_j^{p(c)}k(x_i^p, x_j^p) + \sum_{i=1}^{n_q}\sum_{j=1}^{n_q}\omega_i^{q(c)}\omega_j^{q(c)}k(x_i^q, x_j^q) - 2\sum_{i=1}^{n_p}\sum_{j=1}^{n_q}\omega_i^{p(c)}\omega_j^{q(c)}k(x_i^p, x_j^q)\right],\end{aligned} \tag{3}$$

where p and q are two different distributions, x_i^p $(i = 1, \cdots, n_p)$ and x_j^q $(j = 1, \cdots, n_q)$, respectively, denote the observed samples of distributions p and q, n_p and n_q denote the number of samples of distributions p and q, respectively. $\mathcal{H}$ is the reproducing kernel Hilbert space (RKHS) endowed with a characteristic kernel k, $\phi(\cdot)$ denotes feature map to map the original samples to RKHS, and the kernel k means $k(x^p, x^q) = \langle \phi(x^p), \phi(x^q) \rangle$, where $\langle \cdot, \cdot \rangle$ represents the inner product of two vectors. C is the number of classes, $\omega_i^{p(c)}$ and $\omega_j^{q(c)}$ denote the weights of x_i^p and x_j^q belonging to class c. Note that $\sum_{i=1}^{n_p}\omega_i^{p(c)}$ and $\sum_{j=1}^{n_q}\omega_j^{q(c)}$ are both equal to one, and $\sum_{i=1}^{n}\omega_i^{(c)}\phi(x_i)$ is a

weighted sum on category c. Specifically, we compute $\omega_i^{(c)}$ for sample x_i as

$$\omega_i^{(c)} = \frac{y_{ic}}{\sum_{j=1}^{n} y_{jc}}, \tag{4}$$

where y_{ic} is the c-th element of y_i. For the source samples, the one-hot encoding of the true labels of the samples serves as y_i. In the context of unsupervised domain adaptation, due to the unavailability of labels of target samples, the probability outputs from the source classifier are employed as y_i. Consequently, Eq. (3) can be calculated as the fine-grained domain alignment loss. By minimizing this loss function, the distributions of relevant subdomains within the same category are drawn close [15].

3.4 Two-stage instance selection domain adaptation

To mitigate the domain shift issue and improve the cross-site classification performance of the learned models, we propose TS-ISDA, whose pseudocode is summarized in Algorithm 1. This method could help extract domain-invariant feature representations with the minimum loss of task-related discriminative information. As shown in Figure 1, TS-ISDA consists of three parts: (1) MTD-based source instance selection, (2) target instance refinement, (3) local feature alignment.

Algorithm 1 TS-ISDA.

Require: Labeled source data $\mathcal{D}_s = \{X_s, Y_s\} = \{(x_s^i, y_s^i)\}_{i=1}^{n_s}$; unlabeled target data $\mathcal{D}_t = \{X_t\} = \{(x_t^j)\}_{j=1}^{n_t}$; hyperparameter λ for domain alignment; learning rate α; task networks $F(\cdot;\theta_f)$ and $C(\cdot;\theta_c)$;
Ensure: Optimal weights of task networks θ_f^* and θ_c^*;
1: **for** $k = 1 : N$ **do**
2: Sample a batch of source data $(x_s, y_s) \in \{X_s, Y_s\}$ and a batch of target data $x_t \in X_t$;
3: Calculate the MTD distance between each source instance and the target distribution $d_{mtd}(x_s^i, P(x_t))$, and obtain the selected source domain $\hat{D}_s$ based on the predefined threshold;
4: Calculate local source prototypes $c_s^{(k)}$ $(k = 1, \ldots, K)$ in $\hat{D}_s$, and compute the hard pseudo labels of target samples based on the source classifier;
5: Calculate the cosine distance between each target instance and the source prototype corresponding to its pseudo label, and obtain the selected target domain $\hat{D}_t$;
6: Compute the local subdomain alignment loss $\mathcal{L}_{domain}$ based on $\hat{D}_s$ and $\hat{D}_t$;
7: Compute the classification loss of source data $\mathcal{L}_{cls}$ with (x_s, y_s);
8: Compute the overall loss $\mathcal{L}_{all} = \mathcal{L}_{cls} + \lambda\mathcal{L}_{domain}$;
9: Update the feature extractor $\theta_f \leftarrow \theta_f - \alpha\nabla\mathcal{L}_{all}$ and classifier $\theta_c \leftarrow \theta_c - \alpha\nabla\mathcal{L}_{all}$;
10: **end for**
11: Return θ_f as θ_f^*, θ_c as θ_c^*;

3.4.1 *MTD-based source instance selection*

To avoid negative transfer in the domain adaptation process, we firstly calculate the MTD distance between each source instance and the target distribution, then discard source instances with distances larger than the predefined threshold. The source instance selection function is formulated as follows:

$$\forall\,(x_s^i, y_s^i) \in \mathcal{D}_s\,,\ v_i = \begin{cases} 1, & \text{if } d_{mtd}(x_s^i, P(X_t)) < \tau, \\ 0, & \text{if } d_{mtd}(x_s^i, P(X_t)) \geqslant \tau, \end{cases} \tag{5}$$

where τ denotes the predefined distance threshold, $v_i = 1$ indicates (x_s^i, y_s^i) to be selected, and $v_i = 0$ indicates (x_s^i, y_s^i) not to be selected. After this process, we obtain the selected source domain $\hat{D}_s = \{(x_s^i, y_s^i)\}_{i=1}^{\hat{n}_s}$, where $\hat{n}_s$ denotes the number of selected source samples.

3.4.2 *Target instance refinement*

As is known from the above section, the calculation process of local subdomain alignment loss takes the soft pseudo labels of target samples generated by the source classifier as input. Therefore, target samples with low-quality pseudo labels would misguide the domain alignment process, so it is critical to perform target instance refinement prior to the feature alignment process. Since the labels are available for source samples, we could compute the source prototypes $c_s^{(k)}$ for class k $(k = 1, \ldots, K)$ based on the selected source data. The source prototypes are the mean features of the source samples within the same class, which are calculated as follows:

$$c_s^{(k)} = \frac{1}{N_s^{(k)}} \sum_{(x_s^i, y_s^i) \in \hat{D}_s^{(k)}} F(x_s^i; \theta_f), \tag{6}$$

where $F(\cdot;\theta_f)$ denotes the feature extractor with trainable parameters θ_f, $\hat{D}_s^{(k)}$ represents the set of samples labeled with class k in the selected source domain, $N_s^{(k)}$ is the number of samples in $\hat{D}_s^{(k)}$. Then, a set of prototypes is obtained. It is obvious that target samples with low-quality pseudo labels should gather around the source decision boundary, and are far from the source prototypes corresponding to their pseudo labels. Therefore, we can perform target instance refinement based on the distances between target samples and the corresponding source prototypes. After this process, we can obtain a set of target samples with reliable pseudo labels. Specifically, we firstly calculate the hard pseudo labels of target samples, which are formulated as follows:

$$\hat{y}_t^i = \arg\max C(F(x_t^i;\theta_f);\theta_c), \tag{7}$$

where $C(\cdot;\theta_c)$ denotes the classifier with trainable parameters θ_c, and $\hat{y}_t^i$ is the hard pseudo label of target sample x_t^i. Then, the distance between target sample x_t^i and the corresponding source prototype is calculated as follows:

$$\psi(x_t^i) = d_{cos}(F(x_t^i;\theta_f), c_s^{(\hat{y}_t^i+1)}), \tag{8}$$

where $d_{cos}(\cdot,\cdot)$ denotes the cosine distance between two vectors, $\psi(x_t^i)$ is the distance between x_t^i and the corresponding source prototype.

To obtain a set of target samples with high-quality pseudo labels for category-level domain alignment, we discard target samples exhibiting larger distances. Then, we obtain the selected target domain $\hat{D}_t$.

3.4.3 *Local feature alignment*

According to previous domain adaptation studies [14, 15], the overall loss function is usually composed of classification loss and domain alignment loss. Based on the selected source domain $\hat{D}_s$ and target domain $\hat{D}_t$, the local subdomain alignment loss $\mathcal{L}_{lmmd}$ is formulated as follows:

$$\mathcal{L}_{lmmd} = \hat{d}_{\mathcal{H}}^l(P(\hat{X}_s), P(\hat{X}_t)), \tag{9}$$

where $P(\hat{X}_s)$ and $P(\hat{X}_t)$ denote the feature distributions of the selected source and target data, respectively.

To better mitigate the distribution shift between the source domain and target domain, we can calculate the local subdomain alignment loss at several layers. And the progressive instance selection operations are performed independently at each layer. For example, when the feature alignment process is performed at L layers, the total domain alignment loss $\mathcal{L}_{domain}$ is formulated as follows:

$$\mathcal{L}_{domain} = \sum_{l=1}^{L} \hat{d}_{\mathcal{H}}^l(P(\hat{X}_s^l), P(\hat{X}_t^l)), \tag{10}$$

where $P(\hat{X}_s^l)$ and $P(\hat{X}_t^l)$ denote the feature distributions of the selected source and target data within the l-th $(l = 1, \ldots, L)$ layer, respectively.

3.5 Optimization objective

Due to the availability of source true labels, the classification loss converges rapidly during the training process. In that case, the trained models tend to overfit the source samples, resulting in degraded classification performance in the target domain. Empirically, we find that a non-saturated source classifier is critical to knowledge transfer. According to [20], we add a temperature variate T $(T > 1)$ to the softmax function, and the classification loss is calculated as follows:

$$\mathcal{L}_{cls} = \mathcal{L}_{ce}(softmax(C(F(X_s;\theta_f);\theta_c)/T), Y_s), \tag{11}$$

where $\mathcal{L}_{ce}(\cdot,\cdot)$ denotes the cross-entropy loss function.

In TS-ISDA, the MTD-based source instance selection and target instance refinement steps are performed progressively before calculating the domain alignment loss. The overall loss function is composed of two parts: the domain alignment loss and the classification loss, which is formulated as follows:

$$\mathcal{L}_{all} = \mathcal{L}_{cls} + \lambda \mathcal{L}_{domain}, \tag{12}$$

where λ is a trade-off hyperparameter between the domain alignment loss and the classification loss. To avoid noise at the early training stage, we use a similar schedule method with [14] for λ. Specifically, $\lambda = u \cdot (\frac{2}{1+\exp(-10 \cdot p)} - 1)$, where p is the training progress that varies linearly from 0 to 1, and u is set to 0.1 through several experiments.

4 Experiments

4.1 Materials

4.1.1 *Datasets*

We select six sites consisting of fMRI data of 411 SCZ patients and 592 demographically matched normal controls for analysis of SCZ, i.e., the AMU, COBRE, FMMU#I, FMMU#II, PUTH and UCLA datasets. Similarly, we select six sites consisting of fMRI data of 573 MDD patients and 470 normal controls for analysis of MDD, i.e., the AMU, FMMU#I, FMMU#II, SMU, CSU#I and CSU#II datasets. We also select six sites, each containing more than 50 samples, from the publicly open-access multi-site brain MRI database of ASD—autism brain imaging data exchange I (ABIDE I) [23] for analysis of ASD, i.e., the LEUVEN, NYU, UM, USM, YALE and MAX_MUN datasets. Notably, both the LEUVEN and UM sites are mixed from two datasets collected by the same organization at different time to expand the sample size. The six sites consist of 321 ASD patients and 286 healthy controls totally. The detailed information of the included subjects and the selected datasets is illustrated in the supplementary materials. In addition, the acquired fMRI data are preprocessed based on the previously described pipeline [3, 4, 24] with the statistical parametric mapping software package SPM8[1)].

4.1.2 *Functional connectivity measures*

Due to the prohibitively high dimensionality and relatively low signal-to-noise ratio (SNR) of voxel-wise FC, we extract region-based FC features based on two brain functional atlases for subsequent analysis. Specifically, we utilize the automated anatomical labeling (AAL) atlas [25] and the CC200 atlas [26] for brain parcellation. The AAL atlas divides the brain into 116 brain regions based on neuroanatomical characteristics. The CC200 atlas divides the whole brain into 200 brain regions via spatially constrained spectral clustering. We firstly calculate the average time course of voxels within the same region-of-interest (ROI). The Pearson correlation coefficient between each pair of regional averaged time courses is calculated to quantify the functional coupling of neural activities across diverse brain regions. Then we vectorize the values in the upper triangle of the correlation matrices and obtain two FC vectors for each subject. Furthermore, the Fisher r-to-z transformation and z-standardization operations are progressively used for preprocessing of FC vectors according to [4].

4.2 Competing methods

We compare our proposed TS-ISDA with the following domain adaptation algorithms: (1) joint adaptation network (JAN) [27]; (2) deep subdomain adaption network (DSAN) [15]; (3) domain-adversarial neural network (DANN) [14]; (4) multi-adversarial domain adaptation (MADA) [16]; (5) conditional adversarial domain adaptation network (CDAN) [28]; (6) minimum class confusion (MCC) [29]; (7) entropy regularized optimal transport independence criterion (ETIC) [30]; (8) conditional kernel bures (CKB) [17]; (9) adversarial tight match (ATM) [18]; (10) semantic concentration for domain adaptation (SCDA) [31]; (11) adversarial reweighting with α-power maximization (ARPM) [32].

4.3 Experimental settings and evaluation metrics

In the experiment, all the deep networks and domain adaptation techniques are implemented with PyTorch. It is worth noting that TS-ISDA could be utilized in any deep network. We utilize multilayer perceptron (MLP) with three layers as the feature extractor. The size of the first layer depends on the dimension of input features, and the sizes of the second and third layers are both equal to 128. The classifier network is implemented as one fully connected layer. Since MLP is simple and effective, we utilize it as the backbone network for feature extraction, and to validate the effectiveness of TS-ISDA.

For recognized domain adaptation methods, the detailed settings of hyperparameters are consistent with the original articles. We utilize the Adam optimizer with a learning rate of $5e^{-5}$ for model optimization in all the experiments. For training processes that incorporate domain adaptation techniques, the number of training epochs relies on the convergence speed of the loss function. A batch size of 32 is applied to the source data and target data. The temperature variate T is set to 5 in our experiment. In this study, we perform category-level feature alignment across the selected source and target domains at the last two layers of the feature extractor. Due to the different dimensions of input features, the distance thresholds in the source instance selection stage are, respectively, set to 0.6 and 0.55 for the first and second feature layers when utilizing AAL-based FC, and are, respectively, set to 0.5

1) https://www.fil.ion.ucl.ac.uk/spm.

Table 1 Target performance (%) in diagnostic classification of SCZ based on two brain atlases. The → symbol in the table indicates transfer to the corresponding target site, while data from the remaining sites are combined as the source domain. The best results are in bold.

AAL atlas																					
Algorithm	→ AMU			→ COBRE			→ FMMU#I			→ FMMU#II			→ PUTH			→ UCLA			Average		
	ACC	AUC	F1	ACC	AUC	F1	ACC	AUC	F1	ACC	AUC	F1	ACC	AUC	F1	ACC	AUC	F1	ACC	AUC	F1
JAN [27]	82.8	88.3	79.8	72.3	77.5	66.7	79.4	87.5	74.8	77.5	84.3	66.3	79.1	86.8	75.2	69.5	75.4	53.9	76.8	83.3	69.5
DSAN [15]	83.3	89.6	82.2	70.4	79.3	67.7	79.8	87.2	77.0	75.4	83.0	65.8	**82.0**	88.5	**79.3**	71.3	76.0	**54.7**	77.0	83.9	**71.1**
DANN [14]	79.4	82.8	78.8	69.4	74.7	63.7	79.6	85.8	75.7	77.9	82.0	62.9	77.3	82.9	71.8	74.3	73.7	50.5	76.3	80.3	67.3
MADA [16]	79.1	85.3	78.7	69.9	75.1	67.8	76.5	83.7	72.8	73.8	79.2	63.3	77.3	86.3	73.7	70.5	71.1	46.7	74.5	80.1	67.2
CDAN [28]	81.5	88.9	80.5	73.1	79.1	68.2	79.8	87.0	76.2	77.9	84.2	64.0	79.5	88.0	75.9	72.5	75.2	50.3	77.4	83.7	69.2
MCC [29]	77.8	88.4	79.1	**74.8**	**81.3**	**74.1**	75.8	80.9	73.3	72.2	80.0	61.9	79.1	87.1	76.9	67.3	73.7	52.4	74.5	81.9	69.6
ETIC [30]	81.1	87.1	80.2	71.4	71.4	69.1	79.4	83.3	76.1	78.9	79.8	63.3	81.1	82.1	77.5	**74.9**	72.5	49.1	77.8	79.4	69.2
CKB [17]	82.6	88.0	79.7	70.9	77.3	66.5	79.6	86.7	75.3	74.7	80.8	64.1	79.6	86.7	75.3	69.5	**76.1**	52.8	76.2	82.6	68.9
ATM [18]	77.8	86.8	78.0	68.6	77.3	68.0	77.5	84.2	74.3	77.7	80.5	63.8	78.4	86.7	74.6	72.1	71.1	48.8	75.4	81.1	67.9
SCDA [31]	80.4	81.3	80.0	74.3	74.8	72.9	79.1	77.9	76.5	74.0	77.7	65.0	80.5	80.8	78.1	69.3	70.3	54.2	76.3	77.1	**71.1**
ARPM [32]	75.4	81.5	76.5	65.9	71.1	57.7	74.6	77.1	70.5	65.3	66.1	52.6	77.3	81.9	71.9	69.7	69.6	43.2	71.4	74.5	62.1
TS-ISDA	**84.6**	**90.7**	**82.5**	72.3	79.0	67.1	**81.5**	**88.0**	**77.9**	**80.2**	**85.1**	**67.4**	80.9	**88.8**	77.5	72.5	74.7	50.3	**78.7**	**84.4**	70.5
CC200 atlas																					
Algorithm	→ AMU			→ COBRE			→ FMMU#I			→ FMMU#II			→ PUTH			→ UCLA			Average		
	ACC	AUC	F1	ACC	AUC	F1	ACC	AUC	F1	ACC	AUC	F1	ACC	AUC	F1	ACC	AUC	F1	ACC	AUC	F1
JAN [27]	84.3	91.5	81.6	75.6	82.5	70.9	80.7	86.3	76.5	79.8	85.9	72.3	81.3	86.9	78.1	68.3	74.8	53.1	78.3	84.7	72.1
DSAN [15]	84.8	91.9	83.3	78.3	84.7	75.5	80.1	86.3	77.7	77.2	85.4	68.7	80.7	87.6	78.0	69.9	75.9	**54.1**	78.5	85.3	72.9
DANN [14]	83.9	87.3	82.5	75.1	79.4	71.5	75.6	81.7	71.4	74.5	77.6	64.1	79.5	80.6	76.2	72.9	67.2	43.6	76.9	79.0	68.2
MADA [16]	83.9	90.7	82.7	65.9	72.0	58.2	73.4	83.0	70.2	74.0	78.7	61.7	78.4	85.1	75.4	71.5	69.2	43.5	74.5	79.8	65.3
CDAN [28]	86.3	**93.6**	84.7	78.5	**86.8**	73.4	80.5	**87.0**	77.0	80.0	85.9	70.2	80.4	**88.8**	76.5	**75.4**	73.2	50.6	80.2	85.9	72.1
MCC [29]	80.7	88.6	80.2	72.6	79.6	71.6	77.9	84.4	75.3	74.0	82.0	65.0	79.3	85.9	77.5	66.9	74.0	51.2	75.2	82.4	70.1
ETIC [30]	84.1	92.8	82.3	75.8	84.6	74.3	76.2	84.0	70.8	78.4	84.9	64.6	80.5	78.0	76.8	74.9	71.2	41.8	78.3	82.6	68.4
CKB [17]	80.9	88.9	76.6	74.6	83.3	67.4	77.4	84.2	71.8	78.4	82.5	68.1	80.4	85.9	75.6	68.7	72.7	51.6	76.7	82.9	68.5
ATM [18]	81.1	90.2	78.3	70.1	82.0	61.4	75.1	84.3	72.2	80.9	83.8	65.5	77.5	85.9	71.4	73.7	74.5	41.6	76.4	83.4	65.1
SCDA [31]	84.4	84.9	83.7	74.1	72.4	72.4	76.9	78.5	75.2	76.8	78.9	68.6	80.7	80.5	**78.6**	67.5	67.4	50.5	76.7	77.1	71.5
ARPM [32]	70.0	77.2	65.9	63.7	64.8	55.6	69.6	72.8	66.9	69.7	64.9	53.7	74.8	78.8	69.5	67.3	63.2	34.3	69.2	70.3	57.6
TS-ISDA	**87.2**	92.5	**86.2**	**80.0**	84.9	**76.6**	**81.2**	86.7	**78.8**	**83.7**	**88.1**	**74.4**	**81.4**	87.7	78.1	73.9	**76.1**	52.4	**81.2**	**86.0**	**74.4**

and 0.55 for the first and second feature layers when utilizing CC200-based FC. Since the sample numbers of the selected source and target domains need to be identical in our method, the number of selected target samples is equal to the number of selected source samples. It is worth noting that the hyperparameters just require minimal adjustment to be applicable to other general datasets, enhancing the applicability of TS-ISDA.

For each disorder, we conduct inter-site cross validation experiments to fully evaluate the performance of TS-ISDA. Specifically, each site serves as the target domain once while the rest sites are employed as the source domain. For each target site, we repeat the experiment three times and utilize the average accuracy (ACC), area-under-curve (AUC) and F1 score for algorithm comparison.

4.4 Results and analysis

The target performance of different methods with the AAL atlas and CC200 atlas in diagnostic classification of SCZ, MDD and ASD is shown in Tables 1–3. Specifically, in diagnostic classification of SCZ utilizing AAL-based FC, TS-ISDA obtains the average ACC of 78.7% (AUC: 84.4%), which exceeds the ACC of other methods by at least 0.9% (AUC: 0.5%). When FC is extracted based on the CC200 brain atlas, TS-ISDA obtains a competitive average ACC of 81.2% (AUC: 86.0%), which exceeds the ACC of other methods by at least 1.0% (AUC: 0.1%). As can be seen from Table 1, TS-ISDA achieves over 80% ACC on all sites except UCLA, and an average ACC of 81.2% on six sites with the CC200 brain atlas, meeting the clinically diagnostic accuracy threshold of 80.0%.

For diagnostic classification of MDD, TS-ISDA achieves the average ACC of 63.8% using AAL-based FC, which is equal to the ACC of CDAN, and outperforms other methods. TS-ISDA achieves the average AUC of 68.8%, which exceeds the AUC of other methods by at least 0.6%. When using CC200-based FC, TS-ISDA achieves the average ACC of 68.2% (AUC: 72.8%), which exceeds the ACC of other methods by at least 1.5% (AUC: 0.4%). In

Table 2 Target performance (%) in diagnostic classification of MDD based on two brain atlases. The → symbol in the table indicates transfer to the corresponding target site, while data from the remaining sites are combined as the source domain. The best results are in bold.

AAL atlas

Algorithm	→ AMU			→ FMMU#I			→ FMMU#II			→ SMU			→ CSU#I			→ CSU#II			Average		
	ACC	AUC	F1	ACC	AUC	F1	ACC	AUC	F1	ACC	AUC	F1	ACC	AUC	F1	ACC	AUC	F1	ACC	AUC	F1
JAN [27]	59.3	66.0	65.3	68.7	76.6	69.1	59.2	68.3	57.6	69.4	73.1	70.0	62.0	62.3	64.4	52.7	56.0	**51.4**	61.9	67.0	**63.0**
DSAN [15]	61.0	69.0	66.7	68.7	78.4	69.2	59.2	67.1	56.2	66.8	73.9	66.4	61.3	62.4	64.1	54.8	58.2	47.3	62.0	68.2	61.7
DANN [14]	59.5	68.0	64.9	63.8	68.1	61.0	**62.1**	64.1	53.9	66.0	68.7	63.2	60.2	**63.1**	64.2	54.5	52.9	21.8	61.0	64.2	54.8
MADA [16]	63.4	66.7	70.2	62.8	63.8	60.1	59.2	61.8	54.9	69.2	70.3	68.2	58.1	59.5	58.5	52.7	50.4	32.4	60.9	62.1	57.4
CDAN [28]	62.1	65.8	68.4	70.8	79.1	69.9	61.8	**69.3**	**60.4**	69.8	74.1	70.6	61.2	**63.1**	65.5	57.3	57.3	30.2	**63.8**	68.1	60.8
MCC [29]	63.6	**70.6**	70.0	72.1	78.7	72.2	59.5	62.5	54.4	69.5	75.2	70.5	59.6	60.1	64.0	51.6	55.6	38.3	62.6	67.1	61.6
ETIC [30]	63.0	61.5	70.2	69.3	76.3	69.0	61.8	64.9	57.6	67.1	66.9	65.0	59.9	61.4	63.0	57.3	55.3	22.1	63.0	64.4	57.8
CKB [17]	62.1	69.2	68.0	68.0	75.6	69.0	56.5	61.9	54.0	67.1	73.2	67.8	58.6	60.7	61.3	54.8	57.4	50.6	61.2	66.3	61.8
ATM [18]	64.1	66.7	70.7	68.2	72.7	70.0	**62.1**	66.6	56.7	66.0	69.6	64.1	57.4	61.2	58.2	56.6	**61.1**	28.6	62.4	66.3	58.1
SCDA [31]	60.6	62.9	67.2	**73.6**	74.2	**73.6**	56.9	56.4	53.5	68.8	71.6	69.2	61.1	60.4	64.0	51.6	51.4	41.0	62.1	62.8	61.4
ARPM [32]	**65.8**	68.2	**75.4**	65.1	72.2	67.9	58.8	64.9	51.4	65.5	75.5	69.6	60.8	62.4	65.4	**63.8**	55.5	39.3	63.3	66.4	61.5
TS-ISDA	61.9	69.4	67.7	70.3	**80.5**	71.6	**62.1**	67.8	59.4	**70.6**	**76.6**	**71.2**	**63.2**	**63.1**	**67.0**	54.8	55.3	39.9	**63.8**	**68.8**	62.8

CC200 atlas

Algorithm	→ AMU			→ FMMU#I			→ FMMU#II			→ SMU			→ CSU#I			→ CSU#II			Average		
	ACC	AUC	F1	ACC	AUC	F1	ACC	AUC	F1	ACC	AUC	F1	ACC	AUC	F1	ACC	AUC	F1	ACC	AUC	F1
JAN [27]	67.1	78.2	72.4	72.4	80.5	72.7	63.7	70.7	62.8	**72.2**	**78.7**	**73.0**	61.1	64.5	64.2	59.9	59.4	**58.9**	66.1	72.0	**67.3**
DSAN [15]	71.0	78.2	76.5	74.9	81.5	72.7	64.1	70.4	61.6	68.6	77.1	69.3	**62.6**	66.1	64.4	58.8	**60.9**	54.1	66.7	72.4	66.4
DANN [14]	74.5	73.8	80.8	68.7	72.2	64.4	57.2	65.4	57.6	70.5	75.3	71.4	61.2	64.8	62.3	58.1	54.6	44.2	65.0	67.7	63.4
MADA [16]	61.4	64.5	69.7	65.6	73.7	59.1	60.8	61.6	57.1	65.5	65.7	61.9	61.5	65.4	63.4	56.3	54.7	39.4	61.9	64.3	58.4
CDAN [28]	75.2	78.9	80.9	74.4	81.4	70.5	62.1	**71.9**	61.9	68.8	77.7	71.4	61.7	65.2	**65.4**	54.5	53.8	30.6	66.1	71.5	63.5
MCC [29]	70.4	75.0	76.6	70.0	74.8	70.0	62.7	69.0	61.2	69.8	76.2	70.9	58.2	59.4	61.2	54.8	55.3	47.6	64.3	68.3	64.6
ETIC [30]	74.1	74.9	80.4	72.4	72.9	67.4	63.4	71.5	62.7	69.2	60.7	70.6	60.3	64.4	61.5	56.6	55.7	25.6	66.0	66.7	61.4
CKB [17]	63.4	77.1	67.4	70.0	76.9	69.6	62.1	65.6	62.3	69.9	75.9	71.0	61.6	64.2	64.5	58.1	58.7	57.1	64.2	69.7	65.3
ATM [18]	67.8	74.2	73.3	72.1	79.7	69.9	**66.7**	66.2	61.0	65.7	71.2	61.6	58.5	65.4	56.5	54.5	57.7	36.0	64.2	69.1	59.7
SCDA [31]	71.5	73.4	77.1	73.1	72.3	72.0	66.3	68.4	64.4	70.2	69.3	70.3	59.0	59.6	61.1	56.6	56.0	48.5	66.1	66.5	65.6
ARPM [32]	71.2	72.2	79.5	65.9	71.8	65.4	65.0	65.2	64.0	68.8	77.8	71.0	58.0	63.0	60.2	57.3	49.9	33.2	64.4	66.7	62.2
TS-ISDA	**76.3**	**81.0**	**81.6**	**77.3**	**82.0**	**74.5**	65.0	70.6	**64.7**	70.1	77.8	71.0	60.3	**66.5**	61.6	**60.2**	58.6	46.8	**68.2**	**72.8**	66.7

diagnostic classification of ASD, the classification performance using AAL-based FC is 65.8% (AUC: 70.4%), which exceeds the performance of other methods by at least 0.7% (AUC: 1.2%). When using CC200-based FC, TS-ISDA achieves the average ACC of 69.3% (AUC: 73.7%), which exceeds the ACC of other methods by at least 1.3% (AUC: 0.8%).

As can be seen from Tables 1–3, either for SCZ, MDD or ASD, FC extracted based on the AAL atlas or CC200 atlas, TS-ISDA consistently achieves the best performance, demonstrating the superiority and robustness of this method. It can also be noticed that TS-ISDA obtains a more balanced classification performance for healthy people and patients with neuropsychiatric disorders, which is reflected by higher F1 scores. The comparative methods primarily focus on searching for an optimal feature matching method across the source and target domains, ignoring the impact of unrelated source data and target instances with low-quality pseudo labels on category-level domain adaptation. TS-ISDA progressively performs MTD-based source instance selection and target instance refinement, to filter out unrelated source data and target instances with low-quality pseudo labels, to guarantee the effectiveness of the category-level feature alignment process. Therefore, TS-ISDA outperforms other methods in diagnostic classification of SCZ, MDD and ASD.

To evaluate the effectiveness of components that make up TS-ISDA, we design ablation experiments based on SCZ, MDD and ASD data. The ablation study is developed with the AAL brain atlas and the average testing accuracies on six sites are shown in Table 4. It is observed that the domain alignment module improves the target performance of learned models and TS-ISDA achieves the highest average ACC either for SCZ, MDD or ASD, validating the effectiveness of the local feature alignment and the two-stage instance selection modules.

There are some methods that improve the performance of domain alignment by filtering out target instances with low-quality pseudo labels [20, 33]. To evaluate the performance of the proposed target instance refinement module, we conduct comparative experiments on the diagnostic classification tasks of SCZ using the AAL atlas, and the

Table 3 Target performance (%) in diagnostic classification of ASD based on two brain atlases. The → symbol in the table indicates transfer to the corresponding target site, while data from the remaining sites are combined as the source domain. The best results are in bold.

AAL atlas																					
Algorithm	→ LEUVEN			→ NYU			→ UM			→ USM			→ YALE			→ MAX_MUN			Average		
	ACC	AUC	F1	ACC	AUC	F1	ACC	AUC	F1	ACC	AUC	F1	ACC	AUC	F1	ACC	AUC	F1	ACC	AUC	F1
JAN [27]	60.9	67.5	64.1	62.0	64.6	67.1	66.4	72.0	**68.8**	65.0	72.9	63.4	**74.4**	**80.3**	**75.7**	58.5	58.0	62.4	64.5	69.2	66.9
DSAN [15]	65.6	70.3	66.8	61.2	66.1	65.4	64.6	70.8	66.2	65.3	**73.9**	61.3	68.5	72.0	70.2	62.0	62.3	67.2	64.5	69.2	66.2
DANN [14]	62.0	60.5	68.3	60.7	59.0	69.4	59.8	62.5	57.3	68.0	68.0	63.1	64.3	57.1	62.3	62.0	57.3	66.4	62.8	60.7	64.5
MADA [16]	65.1	68.0	**71.4**	62.3	64.2	70.9	59.5	68.3	53.9	64.0	71.8	59.4	70.8	76.1	70.9	62.6	64.0	67.7	64.1	68.7	65.7
CDAN [28]	65.6	67.3	**71.4**	61.6	63.1	72.0	62.8	70.6	59.6	66.3	72.7	61.1	67.3	74.8	69.4	59.1	58.0	65.9	63.8	67.7	66.5
MCC [29]	63.0	68.6	61.6	59.8	62.8	62.0	62.8	69.9	65.1	66.0	73.6	62.0	64.9	69.2	62.1	57.9	58.2	61.1	62.4	67.1	62.3
ETIC [30]	63.0	62.0	68.3	61.1	62.8	70.9	62.5	70.4	56.9	**68.6**	72.0	60.9	66.1	66.1	63.2	**63.7**	59.3	**69.3**	64.2	65.4	64.9
CKB [17]	67.7	**72.2**	69.4	60.1	63.7	63.9	66.2	71.4	67.5	65.7	71.5	63.4	67.3	70.3	67.5	59.1	62.3	61.9	64.3	68.6	65.6
ATM [18]	61.5	65.3	64.8	62.1	63.0	**72.2**	62.1	68.2	59.5	67.3	70.6	59.2	63.1	69.0	55.6	59.6	56.9	64.0	62.6	65.5	62.5
SCDA [31]	64.1	61.4	66.4	64.3	62.6	68.1	**66.9**	66.9	66.8	65.7	66.7	61.5	69.0	68.3	67.1	60.8	61.1	64.9	65.1	64.5	65.8
ARPM [32]	59.9	64.7	68.8	62.3	64.9	71.3	52.4	52.9	42.2	65.7	70.5	61.0	60.1	56.2	45.5	**63.7**	**68.2**	**69.3**	60.7	62.9	59.7
TS-ISDA	**68.2**	71.0	70.1	**64.5**	**66.6**	70.2	66.7	**73.2**	67.5	68.0	73.7	**64.4**	67.3	75.1	70.6	60.2	63.1	66.9	**65.8**	**70.4**	**68.3**
CC200 atlas																					
Algorithm	→ LEUVEN			→ NYU			→ UM			→ USM			→ YALE			→ MAX_MUN			Average		
	ACC	AUC	F1	ACC	AUC	F1	ACC	AUC	F1	ACC	AUC	F1	ACC	AUC	F1	ACC	AUC	F1	ACC	AUC	F1
JAN [27]	66.7	72.7	69.2	65.2	71.5	68.0	69.2	75.5	72.0	69.3	79.3	68.1	**75.0**	78.4	**76.4**	62.6	60.3	66.3	68.0	72.9	70.0
DSAN [15]	69.3	74.0	72.5	65.4	70.0	69.3	68.5	74.7	70.0	70.0	80.4	67.3	66.7	74.8	67.5	60.2	62.0	64.2	66.7	72.6	68.5
DANN [14]	63.0	62.6	69.6	64.3	68.3	70.5	63.4	66.3	64.0	71.9	70.8	68.5	63.1	66.6	61.5	57.9	53.6	59.5	64.0	64.7	65.6
MADA [16]	65.1	67.1	72.6	67.0	**71.6**	74.8	62.1	74.1	54.6	69.6	81.0	66.7	69.0	**79.1**	68.1	58.5	57.3	63.2	65.2	71.7	66.7
CDAN [28]	71.4	75.4	77.7	**67.9**	**71.6**	**75.4**	62.5	72.1	58.7	73.3	80.5	68.0	72.0	77.2	72.8	60.8	60.3	66.2	68.0	72.8	69.8
MCC [29]	67.7	73.5	69.5	62.7	67.2	66.1	67.1	73.1	68.4	70.3	76.0	66.1	65.5	68.6	64.6	57.3	58.6	63.2	65.1	69.5	66.3
ETIC [30]	70.8	69.9	78.1	66.5	67.0	73.9	61.1	72.1	56.1	**73.6**	74.4	69.8	70.8	74.9	67.7	63.7	59.9	**69.8**	67.8	69.7	69.2
CKB [17]	66.7	71.5	70.2	63.8	68.2	67.5	**69.9**	73.5	**73.2**	70.3	80.3	**70.1**	67.3	68.3	67.4	60.8	**63.8**	64.9	66.4	70.9	68.9
ATM [18]	71.4	**75.8**	77.2	62.5	66.4	69.2	57.0	69.3	37.5	72.6	74.3	61.9	69.0	76.2	63.3	56.1	54.9	54.7	64.8	69.5	60.6
SCDA [31]	74.5	73.8	77.6	65.8	65.5	70.0	68.5	66.6	69.3	70.0	70.3	65.4	63.7	64.3	63.1	60.8	58.9	63.5	67.2	66.6	68.2
ARPM [32]	58.9	65.2	69.7	63.8	70.8	75.1	48.5	49.0	33.6	68.0	72.7	61.2	66.1	59.9	62.9	64.3	68.3	68.7	61.6	64.3	61.8
TS-ISDA	**75.0**	74.5	**78.9**	65.6	70.5	72.2	69.2	**77.2**	70.0	71.6	**81.1**	67.9	69.6	77.1	71.8	**64.9**	61.9	69.4	**69.3**	**73.7**	**71.7**

Table 4 Testing accuracies (%) in ablation study based on the AAL brain atlas. The best results are in bold.

LMMD	Two-stage instance selection	Disorder		
		SCZ	MDD	ASD
		77.8	62.5	64.4
✓		78.4	63.1	65.3
✓	✓	**78.7**	**63.8**	**65.8**

Table 5 Target performance using different target instance selection strategies. Method[1] utilizes the prediction probability scores for target instance selection. Method[2] employs the maximum similarity between each target instance and all source prototypes in the feature space for target instance refinement. The → symbol in the table indicates transfer to the corresponding target site, while data from the remaining sites are combined as the source domain. The best results are in bold.

	→ AMU	→ COBRE	→ FMMU#I	→ FMMU#II	→ PUTH	→ UCLA	Average
Method[1] [33]	81.1	**74.3**	79.8	79.8	80.7	**73.1**	78.1
Method[2] [20]	81.1	**74.3**	80.1	78.4	80.5	72.5	77.8
TS-ISDA (ours)	**84.6**	72.3	**81.5**	**80.2**	**80.9**	72.5	**78.7**

results are presented in Table 5. As can be seen from Table 5, TS-ISDA achieves the best target performance, demonstrating the superiority of our proposed target instance refinement module. Moreover, the method using an alternative target instance selection strategy also achieves superior classification performance compared to other domain adaptation algorithms, further demonstrating the effectiveness and robustness of our proposed TS-ISDA framework.

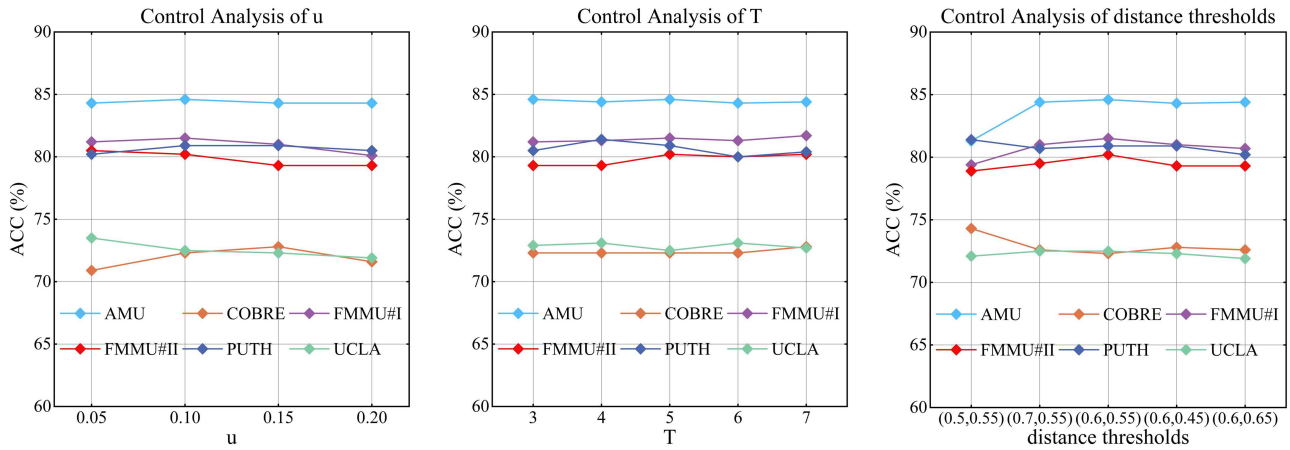


Figure 2 (Color online) Empirical analysis of hyperparameters u, T, and distance thresholds in cross-site diagnostic classification tasks of SCZ with the AAL brain atlas.

Table 6 Testing accuracies (%) with different distance metrics based on the AAL brain atlas. MD: Mahalanobis distance; ED-ave (ED-min, ED-max): average (minimum, maximum) value of the Euclidean distances between the given sample and observed samples of the given distribution. The best results are in bold.

Distance metric	Disorder		
	SCZ	MDD	ASD
MD	78.2	63.2	**65.9**
ED-ave	78.6	62.7	65.4
ED-min	78.3	62.9	65.5
ED-max	78.3	63.6	65.1
MTD (ours)	**78.7**	**63.8**	**65.9**

4.5 Empirical analysis of hyperparameters

In this part, we conduct empirical analysis for hyperparameters u, T and distance thresholds of the two feature layers with the AAL atlas based on multi-site fMRI data of SCZ. Specifically, we firstly keep $T = 5$, distance thresholds = (0.6, 0.55), and vary u between 0.05, 0.1, 0.15, 0.2 to accomplish the diagnostic classification tasks. Secondly, we keep $u = 0.1$, distance thresholds = (0.6, 0.55), and vary T between 1, 3, 5, and 7 to evaluate the target performance of TS-ISDA. Finally, we keep $u = 0.1$, $T = 5$, and vary the distance thresholds between (0.5, 0.55), (0.6, 0.55), (0.7, 0.55), (0.6, 0.45), and (0.6, 0.65) to evaluate the classification performance of TS-ISDA. The classification results using different hyperparameters are presented in Figure 2. As shown in Figure 2, the classification accuracies are relatively stable when choosing different values of hyperparameters. This indicates that TS-ISDA could enhance the target performance of learned models effectively, and is robust to the hyperparameters.

4.6 Analysis of MTD

4.6.1 *Comparison between MTD and other distance metrics*

During the source instance selection process, the MTD distance between each source instance and the target distribution is calculated to measure the transferability of this instance. In order to demonstrate the superiority of MTD compared to other sample-distribution distance measurement methods, we conduct comparative experiments based on the AAL atlas, in which MTD is replaced by four distance metrics while the rest experimental settings remain unchanged. To ensure the fairness of the comparison, we discard 20% of the source and target instances with larger distances in each experiment. The average accuracies on six sites using different distance metrics are listed in Table 6, where MD denotes Mahalanobis distance, ED-ave, ED-min and ED-max denote the average value, minimum value and maximum value of the Euclidean distances between the given sample and observed samples of the given distribution. As shown in Table 6, MTD consistently outperforms other distance metrics in diagnostic classification of SCZ, MDD and ASD, which further illustrates the superiority and robustness of MTD. In addition, it is observed that the testing accuracies utilizing other distance metrics exceed ACCs of most competing domain adaptation methods, demonstrating the effectiveness of the proposed two-stage instance selection framework.

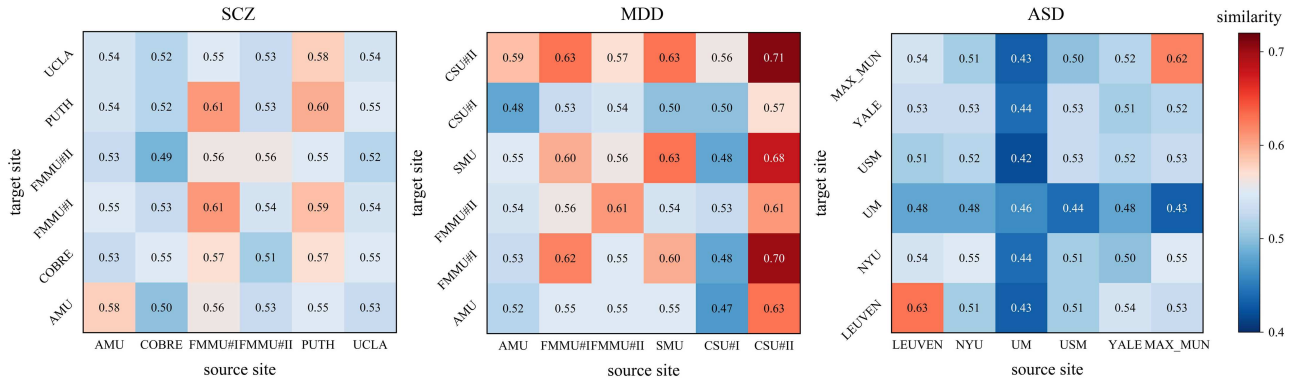


Figure 3 (Color online) MTD-based data heterogeneity analysis across multiple sites of SCZ, MDD and ASD. FCs extracted based on the AAL brain atlas are utilized as the features of samples. The inter-site similarity is derived by calculating the average value of the MTD-based similarities between samples in the source site and the distribution characterized by samples in the target site. The self-similarity of one site is derived by averaging the MTD-based similarities between each sample in this site and the distribution characterized by the rest samples.

4.6.2 *MTD-based inter-site data heterogeneity analysis*

To validate the existence of inter-site distribution differences and demonstrate the effectiveness of MTD in sample-distribution distance measurement, we conduct data heterogeneity analysis across different sites based on MTD. Specifically, since similarity is negatively correlated with distance and generally ranges between 0 and 1, we derive the similarity between sample x_m and distribution $P(X_d)$ according to the following equation:

$$Sim(x_m, P(X_d)) = 1 - \frac{1}{1 + \exp(-10 \cdot (d_{mtd}(x_m, P(X_d)) - u))}, \tag{13}$$

where u is utilized to adjust the scale of the similarity, and is set to 0.75 in our experiment; $Sim(x_m, P(X_d))$ denotes the similarity between sample x_m and distribution $P(X_d)$. We calculate the average value of the similarities between samples in the source site and the distribution characterized by samples in the target site. We also calculate the average value of the intra-site similarities derived using the leave-one-out strategy in the target site. Specifically, the intra-site similarity of one target sample is defined as the similarity between this sample and the distribution characterized by the rest samples in the target site. FCs extracted based on the AAL atlas are directly utilized as features of the samples, and this process is independently performed on the aforementioned six SCZ sites, six MDD sites and six ASD sites. Figure 3 depicts the similarity analysis results based on multi-site fMRI data of SCZ, MDD and ASD. As shown in Figure 3, either for SCZ, MDD or ASD, samples from the target site are generally more similar to the target distribution compared to samples from other sites, as reflected in Figure 3, where the values on the subdiagonal line are generally larger than other values on the same line. As mentioned previously, different sites usually suffer from distribution differences caused by different data distributions. Our conclusion is consistent with this statement, as well as demonstrating the effectiveness of MTD in sample-distribution distance measurement to some extent. In addition, we can also derive the similarity relationships between different sites from Figure 3. For six MDD sites, CSU#I exhibits low similarity with other sites while CSU#II exhibits high similarity with other sites. For six ASD sites selected from the ABIDE I database, the inter-site distribution differences are relatively large compared to multiple SCZ and MDD sites, and UM exhibits significantly low similarity with other sites among the six ASD sites.

4.7 Visualization of feature distributions

To evaluate the effectiveness of TS-ISDA in mitigating the distribution shift across the source and target domains, we utilize the t-SNE project [34] for visualization in Figure 4. The FCs are extracted based on the AAL atlas, and we visualize the feature distributions within two feature layers of MLP and TS-ISDA based on SCZ, MDD and ASD data. For the analysis of SCZ, MDD and ASD, the AMU, AMU and LEUVEN datasets serve as the target domain while the rest sites are mixed as the source domain. As shown in Figure 4, significant feature distribution differences exist between the source domain and target domain, and the feature representations of different classes in the target domain are mixed when using MLP for feature extraction. In comparison, TS-ISDA could align the class-level feature distributions across the source and target domains, and promote the inter-class separation of feature representations in the target domain. Hence the learned models could generalize to the target domain well.

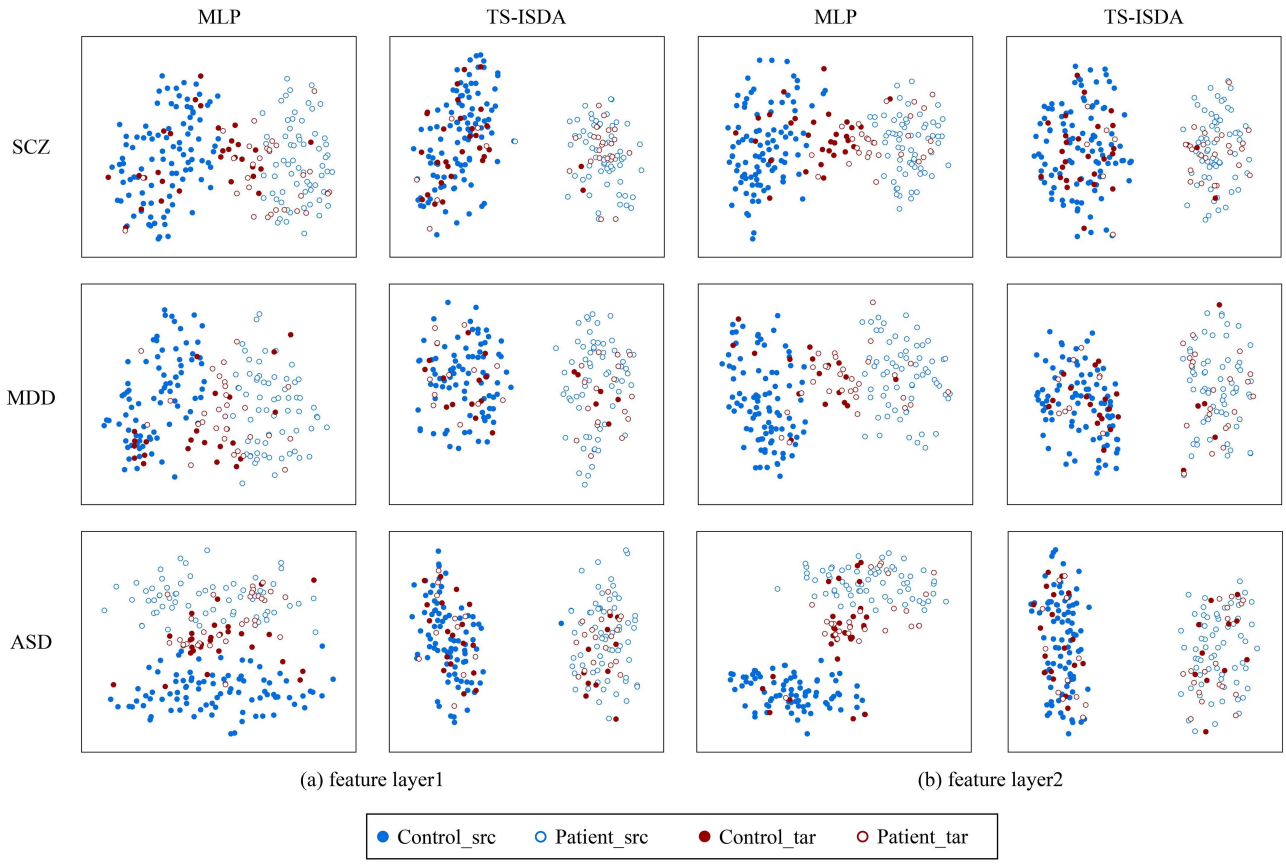


Figure 4 (Color online) Visualization of feature distributions within two feature layers of MLP and TS-ISDA using t-SNE projection [34] based on the AAL brain atlas. For the analysis of SCZ, MDD and ASD, the AMU, AMU and LEUVEN datasets serve as the target domain while the remaining sites are mixed as the source domain. Note that Control_src and Patient_src represent healthy controls and patients with neuropsychiatric disorders in the source domain, respectively. The Control_tar and Patient_tar denote healthy controls and patients with neuropsychiatric disorders in the target domain, respectively.

4.8 Discriminative FCs and brain regions

To localize the biological markers associated with neuropsychiatric disorders and validate the biological interpretability of TS-ISDA, we visualize the most discriminative FCs and brain regions based on the AAL atlas. Firstly, the weights of different FCs and brain regions are derived utilizing the canonical correlation analysis (CCA) according to [35]. The FCs with the top 100 highest weights and the brain regions with the top 20 highest weights are considered discriminative in diagnosing neuropsychiatric disorders. Based on the different functions, the brain regions can be grouped into six functional networks, i.e., the FPN (frontoparietal control network), Visual, DMN (default mode network), SMN (sensorimotor network), SubCort (subcortical area) and CER (cerebellum). It is worth noting that the weights of different functional networks are influenced heavily by the number of included brain regions; thus we identify discriminative functional networks based on the number of discriminative brain regions that they include.

Figure 5(a) depicts the discriminative FCs and brain regions that contribute most in diagnostic classification of SCZ. It is observed that the right inferior orbitofrontal cortex (ORBinf), the inferior frontal gyrus (IFG), the supplementary motor area (SMA), the left postcentral gyrus (PoCG), the lenticular nucleus putamen (PUT) and the middle temporal gyrus (MTG) regions are critical in the classification of SCZ, which is consistent with previous studies [36–38]. We can also notice that the abnormal dysconnectivity patterns exist between FPN and SMN, and between FPN and SubCort. When observing the functional networks, the SubCort and DMN consist of the most discriminative brain regions. In summary, the most discriminative brain regions and FCs associated with SCZ are closely linked to emotion processing, personality traits and hearing, reflecting the widely recognized functional deficits in SCZ patients.

Figure 5(b) depicts the discriminative FCs and brain regions that exhibit the strongest correlation with the anomaly scores in diagnostic classification of MDD. It is evident that the orbitofrontal cortex (ORB), the gyrus rectus (REC), the left hippocampus (HIP), the parahippocampal gyrus (PHG), the thalamus (THA), the right

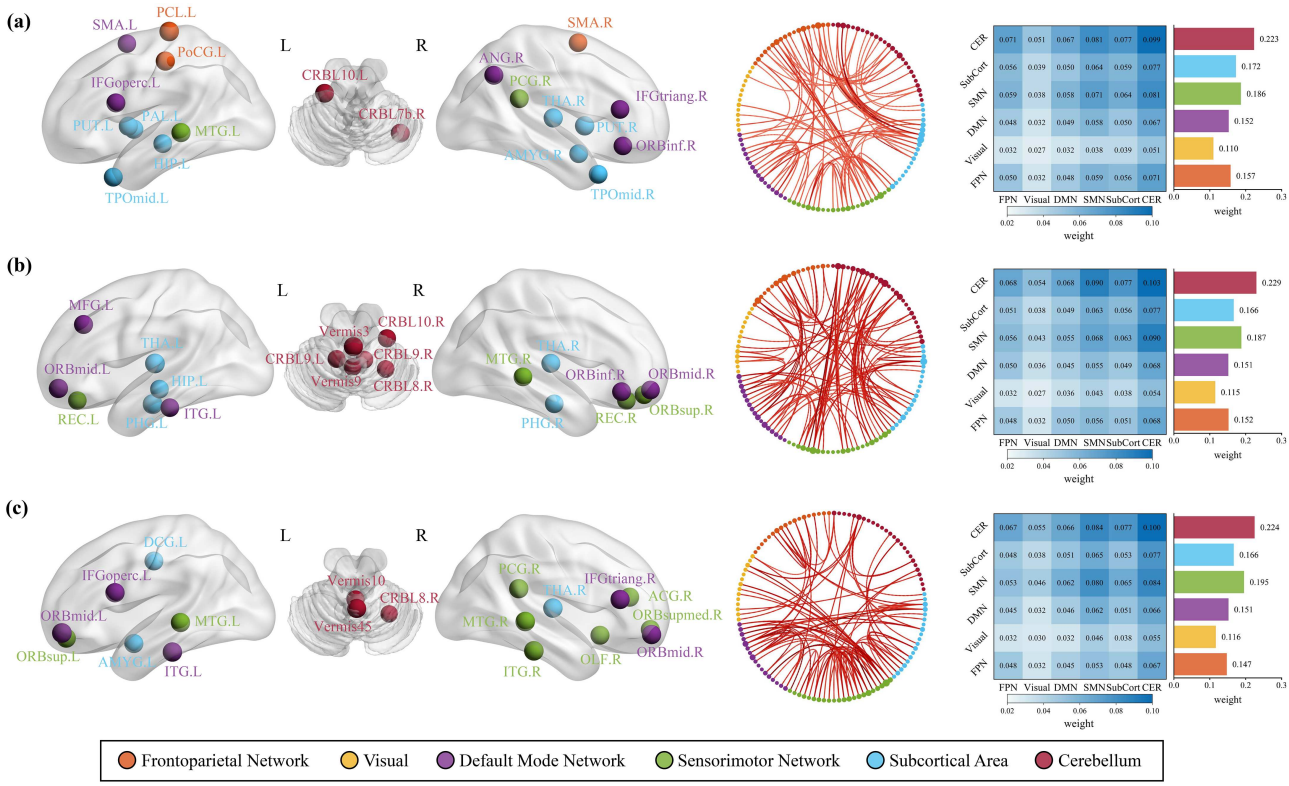


Figure 5 (Color online) Discriminative FC and brain regions identified by TS-ISDA using the AAL atlas in diagnostic classification of SCZ (a), MDD (b) and ASD (c). The nodes are colored to represent different functional networks. We visualize the top 20 brain regions and top 100 FCs that contribute most to the classification anomaly scores. The FC weights between different functional networks are also calculated to help identify functional networks that contribute significantly to the diagnosis of neuropsychiatric disorders.

MTG, the left inferior temporal gyrus (ITG) and the cerebellum regions play important roles in classification of MDD, which aligns with previous studies [39–42]. We can also note that significant dysconnectivity patterns exist between CER and SMN. When observing the functional networks, the CER and DMN consist of the most discriminative brain regions. In summary, the most discriminative brain regions and FCs associated with MDD are closely linked to emotion regulation, cognitive function and memory, reflecting the widely recognized functional deficits in patients with MDD.

Figure 5(c) depicts the discriminative FCs and brain regions that exhibit the highest correlation with the anomaly scores in diagnostic classification of ASD. It is obvious that the middle orbitofrontal cortex (ORBmid), the paracingulate gyri (PCG), the left Amygdala (AMYG), the MTG, the inferior temporal gyrus (ITG) and the cerebellum regions are critical in the classification of ASD, which is consistent with previous studies [43–45]. We can also notice that significant dysconnectivity patterns exist between DMN and SubCort, and within SMN. When observing the functional networks, the SMN and DMN consist of the most discriminative brain regions. In summary, the most discriminative brain regions and FCs associated with ASD are closely linked to social behavior, language function and affective expression, reflecting the widely recognized functional deficits in patients with ASD.

Considering three different neuropsychiatric disorders, we notice that the ORB and the MTG regions consistently contribute significantly to the diagnostic classification of SCZ, MDD and ASD. When observing the functional networks, we note that DMN is critical for the diagnostic classification of these three neuropsychiatric disorders. DMN is closely related to self-cognition, emotion regulation and memory, which aligns with the typical symptoms of patients with SCZ, MDD and ASD. This finding reveals the biological etiological homogeneity across different neuropsychiatric disorders and, to some extent, explains the overlapping symptomatic manifestations observed in patients with SCZ, MDD, and ASD, which is consistent with previous studies [35, 42, 46].

5 Conclusion

In this study, we propose the minimum transfer distance to measure the distance between the given sample and distribution. Based on MTD, we also propose a two-stage instance selection domain adaptation algorithm for fMRI-

based cross-site diagnostic classification of neuropsychiatric disorders. TS-ISDA could help avoid negative transfer in the domain adaptation process, and select target instances with high-quality pseudo labels for effective and appropriate fine-grained domain alignment, thus enhancing the target performance of learned models. Specifically, the MTD-based source instance selection and the target instance refinement steps are performed progressively to filter out unrelated source data and target instances with low-quality pseudo labels. Afterwards, the category-level feature alignment process is carried out on the selected source and target data. We conduct a large-scale cross-site diagnostic classification study of SCZ, MDD and ASD with the AAL and CC200 brain atlases. Experimental results show that TS-ISDA achieves the average ACCs of 81.2%, 68.2% and 69.3% with the CC200 atlas in diagnostic classification of SCZ, MDD and ASD, respectively, outperforming state-of-the-art methods. Furthermore, we also localize disorder-associated discriminative FCs and brain regions, and find that the ORB and MTG regions consistently play a significant role in the diagnostic classification of SCZ, MDD and ASD, revealing the homogeneity in the pathogenesis of various neuropsychiatric disorders.

Acknowledgements This work was supported by National Natural Science Foundation of China (Grant Nos. U24A20339, T2521006), Brain Science and Brain-like Intelligence Technology-National Science and Technology Major Project (Grant No. 2022ZD0208903), Scientific Research Innovation Capability Support Project for Young Faculty (Grant No. SRICSPYF-BS2025012), and Science and Technology Innovation Program of Hunan Province (Grant Nos. 2023RC1004, 2024QK2006).

Supporting information Appendixes A and B. The supporting information is available online at info.scichina.com and link.springer.com. The supporting materials are published as submitted, without typesetting or editing. The responsibility for scientific accuracy and content remains entirely with the authors.

References

1 Kanter J W, Busch A M, Weeks C E, et al. The nature of clinical depression: symptoms, syndromes, and behavior analysis. Behav Analyst, 2008, 31: 1–21
2 Zeng L L, Shen H, Liu L, et al. Identifying major depression using whole-brain functional connectivity: a multivariate pattern analysis. Brain, 2012, 135: 1498–1507
3 Zeng L L, Shen H, Liu L, et al. Unsupervised classification of major depression using functional connectivity MRI. Hum Brain Mapping, 2014, 35: 1630–1641
4 Zeng L L, Wang H, Hu P, et al. Multi-site diagnostic classification of schizophrenia using discriminant deep learning with functional connectivity MRI. eBioMedicine, 2018, 30: 74–85
5 Guan H, Liu M. Domain adaptation for medical image analysis: a survey. IEEE Trans Biomed Eng, 2021, 69: 1173–1185
6 Wang J, Zhang L, Wang Q, et al. Multi-class ASD classification based on functional connectivity and functional correlation tensor via multi-source domain adaptation and multi-view sparse representation. IEEE Trans Med Imag, 2020, 39: 3137–3147
7 Kunda M, Zhou S, Gong G, et al. Improving multi-site autism classification via site-dependence minimization and second-order functional connectivity. IEEE Trans Med Imag, 2023, 42: 55–65
8 Huang Y L, Hsieh W T, Yang H C, et al. Conditional domain adversarial transfer for robust cross-site ADHD classification using functional MRI. In: Proceedings of the IEEE International Conference on Acoustics, Speech, and Signal Processing, 2020. 1190–1194
9 Wang Z R, Dai Z H, Póczos B, et al. Characterizing and avoiding negative transfer. In: Proceedings of the IEEE Conference on Computer Vision and Pattern Recognition (CVPR), 2019. 11285–11294
10 Zhang J, Ding Z W, Li W Q, et al. Importance weighted adversarial nets for partial domain adaptation. In: Proceedings of the IEEE Conference on Computer Vision and Pattern Recognition (CVPR), 2018. 8156–8164
11 Azarkesht M, Afsari F. Instance reweighting and dynamic distribution alignment for domain adaptation. J Ambient Intell Hum Comput, 2022, 13: 4967–4987
12 Li H, He F, Pan Y. Multi-objective dynamic distribution adaptation with instance reweighting for transfer feature learning. Knowledge-Based Syst, 2023, 263: 110303
13 Long M S, Cao Y, Wang J M, et al. Learning transferable features with deep adaptation networks. In: Proceedings of the 32nd International Conference on Machine Learning (ICML), 2015. 97–105
14 Ganin Y, Lempitsky V. Unsupervised domain adaptation by backpropagation. In: Proceedings of the 32nd International Conference on Machine Learning (ICML), 2015. 1180–1189
15 Zhu Y, Zhuang F, Wang J, et al. Deep subdomain adaptation network for image classification. IEEE Trans Neural Netw Learn Syst, 2021, 32: 1713–1722
16 Pei Z Y, Cao Z J, Long M S, et al. Multi-adversarial domain adaptation. In: Proceedings of the 32nd AAAI Conference on Artificial Intelligence, 2018. 3934–3941
17 Luo Y W, Ren C X. Conditional bures metric for domain adaptation. In: Proceedings of the IEEE Conference on Computer Vision and Pattern Recognition (CVPR), 2021. 13984–13993
18 Li J, Chen E, Ding Z, et al. Maximum density divergence for domain adaptation. IEEE Trans Pattern Anal Mach Intell, 2021, 43: 3918–3930
19 Kang G, Jiang L, Wei Y, et al. Contrastive adaptation network for single- and multi-source domain adaptation. IEEE Trans Pattern Anal Mach Intell, 2022, 44: 1793–1804
20 Chen C Q, Xie W P, Huang W B, et al. Progressive feature alignment for unsupervised domain adaptation. In: Proceedings of the IEEE Conference on Computer Vision and Pattern Recognition (CVPR), 2019. 627–636
21 Tang Y, Tong G, Xiong X, et al. Multi-site diagnostic classification of Autism spectrum disorder using adversarial deep learning on resting-state fMRI. BioMed Signal Processing Control, 2023, 85: 104892
22 Zhang L, Wang J R, Ma Y. Graph convolutional networks via low-rank subspace for multi-site rs-fMRI asd diagnosis. In: Proceedings of the International Congress on Image and Signal Processing, BioMedical Engineering and Informatics (CISP-BMEI), 2021. 1–6
23 Di Martino A, Yan C G, Li Q, et al. The autism brain imaging data exchange: towards a large-scale evaluation of the intrinsic brain architecture in autism. Mol Psychiatry, 2014, 19: 659–667
24 Su J, Wang B, Fan Z, et al. M^2DC: a meta-learning framework for generalizable diagnostic classification of major depressive disorder. IEEE Trans Med Imag, 2025, 44: 855–867
25 Tzourio-Mazoyer N, Landeau B, Papathanassiou D, et al. Automated anatomical labeling of activations in SPM using a macroscopic anatomical parcellation of the MNI MRI single-subject brain. NeuroImage, 2002, 15: 273–289
26 Craddock R C, James G A, Holtzheimer III P E, et al. A whole brain fMRI atlas generated via spatially constrained spectral clustering. Hum Brain Mapping, 2012, 33: 1914–1928

27 Long M S, Zhu H, Wang J M, et al. Deep transfer learning with joint adaptation networks. In: Proceedings of the 34th International Conference on Machine Learning (ICML), 2017. 2208–2217
28 Long M S, Cao Z J, Wang J M, et al. Conditional adversarial domain adaptation. In: Proceedings of the Advances in Neural Information Processing Systems 31 (NeurIPS), 2018. 1647–1657
29 Jin Y, Wang X M, Long M S, et al. Minimum class confusion for versatile domain adaptation. In: Proceedings of the 18th European Conference on Computer Vision (ECCV), 2020. 464–480
30 Liu L, Pal S, Harchaoui Z. Entropy regularized optimal transport independence criterion. In: Proceedings of the International Conference on Artificial Intelligence and Statistics, 2022. 11247–11279
31 Li S, Xie M X, Lv F R, et al. Semantic concentration for domain adaptation. In: Proceedings of the IEEE International Conference on Computer Vision, 2021. 9102–9111
32 Gu X, Yu X, Yang Y, et al. Adversarial reweighting with α-power maximization for domain adaptation. Int J Comput Vis, 2024, 132: 4768–4791
33 Hu Y, Huang Z-A, Liu R, et al. Source free semi-supervised transfer learning for diagnosis of mental disorders on fMRI scans. IEEE Trans Pattern Anal Mach Intell, 2023, 45: 13778–13795
34 van der Maaten L, Hinton G. Visualizing data using t-SNE. J Mach Learn Res, 2008, 9: 2579–2605
35 Su J, Shen H, Peng L, et al. Few-shot domain-adaptive anomaly detection for cross-site brain images. IEEE Trans Pattern Anal Mach Intell, 2024, 46: 1819–1835
36 Boisvert M, Lungu O, Pilon F, et al. Regional cerebral blood flow at rest in schizophrenia and major depressive disorder: A functional neuroimaging meta-analysis. Psychiatry Res-NeuroImag, 2023, 335: 111720
37 Jing H, Zhang C, Yan H, et al. Deviant spontaneous neural activity as a potential early-response predictor for therapeutic interventions in patients with schizophrenia. Front Neurosci, 2023, 17: 1243168
38 Picó-Pérez M, Vieira R, Fernández-Rodríguez M, et al. Multimodal meta-analysis of structural gray matter, neurocognitive and social cognitive fMRI findings in schizophrenia patients. Psychol Med, 2022, 52: 614–624
39 Ahn S J, Kyeong S, Suh S H, et al. What is the impact of child abuse on gray matter abnormalities in individuals with major depressive disorder: a case control study. BMC Psychiatry, 2016, 16: 397
40 Hao H H, Chen C, Mao W B, et al. Aberrant brain regional homogeneity in first-episode drug-naïve patients with major depressive disorder: a voxel-wise meta-analysis. J Affective Disord, 2018, 245: 63–71
41 Li N, Jin D, Wei J, et al. Functional brain abnormalities in major depressive disorder using a multiscale community detection approach. Neuroscience, 2022, 501: 1–10
42 Zeng L L, Fan Z, Su J, et al. Gradient matching federated domain adaptation for brain image classification. IEEE Trans Neural Netw Learn Syst, 2024, 35: 7405–7419
43 Weston C S E. Four social brain regions, their dysfunctions, and sequelae, extensively explain autism spectrum disorder symptomatology. Brain Sci, 2019, 9: 6
44 Cai J, Hu X, Guo K, et al. Increased left inferior temporal gyrus was found in both low function autism and high function autism. Front Psychiatry, 2018, 9: 542
45 Sherkatghanad Z, Akhondzadeh M, Salari S, et al. Automated detection of autism spectrum disorder using a convolutional neural network. Front Neurosci, 2020, 13: 1325
46 Dai M, Su J, Fan Z, et al. Feature and semantic matching multisource domain adaptation for diagnostic classification of neuropsychiatric disorders. IEEE Trans Cogn Dev Syst, 2025, 17: 1474–1487